Hindawi Publishing Corporation
International Journal of Chemical Engineering
Volume 2015, Article ID 795386, 7 pages
http://dx.doi.org/10.1155/2015/795386

Research Article

A Study of CO_2 Methanation over Ni-Based Catalysts Supported by CNTs with Various Textural Characteristics

Yanyan Feng,[1,2] Wen Yang,[1,2] and Wei Chu[2]

[1]*Department of Chemistry and Bioengineering, Guilin University of Technology, Guilin 541006, China*
[2]*Department of Chemical Engineering, Sichuan University, Chengdu 610065, China*

Correspondence should be addressed to Wei Chu; chu1965chengdu@163.com

Received 18 July 2015; Revised 15 September 2015; Accepted 29 September 2015

Academic Editor: Moshe Sheintuch

This work studied the influence of textural characteristics of CNTs on catalytic performance of Ni/CNTs for CO_2 methanation. The CNTs supports were prepared by chemical vapor deposition method using Ni/MgO catalysts, and acetonitrile and ethanol were used as carbon sources, respectively. The Ni/CNTs catalysts were prepared via impregnation method and characterized by X-ray diffraction (XRD), N_2 adsorption/desorption, and temperature-programmed reduction (H_2-TPR) techniques. The results indicated that the textural characteristics of CNTs supports significantly impacted on the catalytic performance of Ni/CNTs. The catalyst Ni/CNTs-E (CNTs using ethanol as carbon source) had good reducibility, high specific surface area, and moderate defects, resulting in higher CO_2 conversion and CH_4 yield, followed by Ni/CNTs-C (commercial CNTs) and Ni/CNTs-A (CNTs using acetonitrile as carbon source). Based on Arrhenius formula, activation energies of the catalysts were calculated and were found decreased for Ni/CNTs-A and Ni/CNTs-E.

1. Introduction

CO_2 emissions increased dramatically due to human activities, including power generation, transportation, deforestation, and fossil fuels [1–3]. The CO_2 recycling has become an important topic in recent years, and a lot of researches have been conducted [4–6]. As CO_2 is one of the main contributors to greenhouse effect and hence to climate change, there is a growing interest in its use as a feedstock in chemical processes [3, 7], wherein CO_2 capture and storage (CCS) and CO_2 chemical conversion [8] have attracted wide interests. It is important to convert CO_2 to fuels or raw materials which must be also easily transportable. CH_4 is suitable for this because it benefits from the existing infrastructure for transport and storage of natural gas [9–11].

CO_2 methanation ($CO_2 + 4H_2 \rightarrow CH_4 + 2H_2O$) is one of the most important methods and has been studied extensively using different types of metals and supports [3, 12]. The CO_2 methanation reaction is exothermic, and an eight-electron process is required to reduce the fully oxidized carbon to CH_4 with an appropriate catalyst. Ni [1, 13–16], Ru [2, 3], and Rh [7, 12, 17, 18] based catalysts have been proved to have good catalyst activities in CO_2 methanation [19], and nickel based catalysts have been extensively investigated under varying experimental conditions for its low price and high activity. Currently, main supports of the catalysts are activated carbon (AC) [18], Al_2O_3 [7, 17, 18], SiO_2, ZrO_2 [1, 13, 16], molecular sieve, Ni/$Ce_xZr_{1-x}O_2$ [5], TiO_2 [12], SiC [15], and CeO_2 [20].

Carbon nanotubes (CNTs), as a novel nano-carbon catalyst support, have been widely used due to their interesting mechanical and electronic properties and stability [21–23]. The enhanced activity of CNTs systems has been attributed to an electronic interaction between the metal and the support, as well as the overflow effect of hydrogen [24, 25]. The effect of CNTs with various textural characteristics and defects has not been studied in detail for CO_2 methanation. It has been shown that in the case of catalysts supported by CNTs with high specific surface area, highly dispersed metal of small particles was easily formed and more active than large metal ensembles. For catalysts supported by CNTs with more defects, it was advantageous to promote the metal loading and the dispersion of active components.

The present work aimed to clarify some aspects of the activity of nickel based catalysts supported by CNTs with various textural characteristics toward CO_2 methanation. The objective was to study the effect of textural characteristics on the catalysts and their catalytic activity for CO_2 methanation at different temperatures. The synthesized catalysts were characterized by X-ray diffraction (XRD), N_2 adsorption/desorption, and temperature-programmed reduction (H_2-TPR) techniques, respectively.

2. Experimental

2.1. Catalysts Preparation. The CNTs supports were prepared by chemical vapor deposition (CVD) method using Ni/MgO catalysts, and acetonitrile and ethanol were used as carbon sources, respectively. The Ni/MgO catalyst was prepared by citrate complex method. $Ni(NO_3)_3{\cdot}6H_2O$ and $Mg(NO_3)_2{\cdot}6H_2O$ were mixed in a citric acid aqueous solution, stirred and gelated at 70°C. After drying at 120°C overnight, the dried gel was calcined at 500°C for 3 h in air to get the Ni/MgO catalyst. The loading of Ni on the catalyst was kept at 50 wt.%. To grow CNTs, 100 mg of catalyst powder was dispersed on boat and was then placed in a horizontal quartz reactor. Firstly, the catalyst powder was reduced in situ in H_2 at 550°C for 1 h. Subsequently, the sample was heated to 650°C in flowing N_2 and then bubbled the acetonitrile and ethanol for 1 h. After 1 h of reaction, the obtained CNTs were cooled to room temperature in a N_2 atmosphere. The CNTs were further purified in 100 mL of concentrated HCl at room temperature for 12 h. After purification, the CNTs were filtered and washed with deionized water until the pH of the filtrate was around 7.0. Finally, the product was dried at 100°C overnight and labeled as "CNTs-A" and "CNTs-E," where A and E represented the as-prepared CNTs using acetonitrile and ethanol as carbon source, respectively. For comparison, the commercial CNTs purchased from the Chengdu Organic Chemical Limited Company in China were applied and named as "CNTs-C."

The catalysts Ni/CNTs-A, Ni/CNTs-E, and Ni/CNTs-C were prepared via impregnation method. An aqueous solution of $Ni(NO_3)_2$ was prepared by dissolving 1.19 g $Ni(NO_3)_2{\cdot}6H_2O$ into 4.0 mL H_2O. Next, 1.76 g of CNTs sample was impregnated with the $Ni(NO_3)_2$ solution and stirred at room temperature for 2 h and then evaporated to dryness at an 80°C water bath. The impregnated Ni/CNTs (Ni 12 wt.%) were dried at 110°C for 12 h and calcined in N_2 at 450°C for 3 h. The catalyst Ni/AC (using activated carbon as the support) was prepared with aqueous solution of $Ni(NO_3)_2$ by the same method.

2.2. Catalytic Activity Evaluation. The catalytic activity measurement was conducted under atmospheric pressure in a fixed-bed reactor with an internal diameter of 6 mm. 100 mg of catalyst was loaded into the reactor and reduced with H_2 at 450°C for 1 h prior to catalytic evaluation. The CO_2 methanation reaction was performed at various reaction temperatures using a mixture of H_2 and CO_2 at molar ratio of 4. Effluent gases from the reactor were analyzed online by a SC-200 model gas chromatograph with a TDX-01 column and a thermal conductivity detector (TCD). The length and temperature of column were 2.0 m and 80°C, while the detector temperature was 60°C, and the retention times of H_2, CO, CH_4, and CO_2 were 0.9 min, 2.5 min, 6.0 min, and 10.5 min, respectively.

2.3. Characterization. N_2 adsorption/desorption isotherms were measured at 77 K with a Quantachrome Nova 1000e apparatus using an automated gas sorption system. Prior to the measurement, the sample was degassed at 120°C for 3 h. The specific surface areas (S_{BET}) of the catalysts were determined using the BET equation, and the total pore volume (V_t) was calculated from the volume of nitrogen held at P/P_0 = 0.98~0.99. Pore size distributions (PSDs) were estimated using the DFT (Density Functional Theory) equation.

The weight change of the sample was determined with a thermogravimetric analyzer (TGA Q500). In this protocol, 10 mg sample in the TGA was kept at room temperature for about 30 min, and then it was heated up to 900°C with a heating rate of 10°C/min in the air.

Raman spectroscopy measurements of the samples were obtained with a Raman microspectrometer (LabRAM HR) that used an argon laser as the excitation (λ = 532 nm). The spectra were recorded in the wave number range of 400–4000 cm^{-1} with typical exposure times of 2 s. During the analysis, at least four tests were performed on different sections of each individual sample.

Phase analysis was performed using power X-ray diffraction (XRD) technique. The X-ray diffraction patterns were carried on X-ray diffraction apparatus (D/MAX-2500, Rigaku Company) with Cu Kα (50 KV, 100 mA) radiation.

Temperature-programmed reduction (H_2-TPR) experiments were carried out in a fixed-bed reactor. 100 mg sample was loaded in the middle of the reactor tube. The temperature of the reactor was raised from 100°C to 800°C at a heating rate of 10°C/min under 5% H_2/95% N_2 with a flow rate of 30 mL/min. The H_2 consumption was analyzed online by a SC-200 gas chromatograph with a thermal conductivity detector (TCD).

3. Results and Discussion

3.1. Characterization of CNTs. Figure 1(a) showed the N_2 adsorption/desorption isotherms obtained on CNTs samples. These isotherms were type III, that is, the obviously increasing uptakes at the high relative pressure values. It was obvious that the isotherms of samples dramatically increased on reaching a relative pressure of unity. The isotherms exhibited remarkable hysteresis loops at higher relative pressure values (P/P_0 > 0.4). Moreover, the adsorption volume of sample CNTs-E was the highest among the three samples, while the adsorption volume of CNTs-A was the lowest. The pore size distribution (PSD) computed with the DFT method was displayed in Figure 1(b). In order to make the graph full scale, the maximum value on the x-axis was 35 nm. The CNTs containing larger pores were produced. The pore diameter range presented in Figure 1(b) was typical of mesoporous materials.

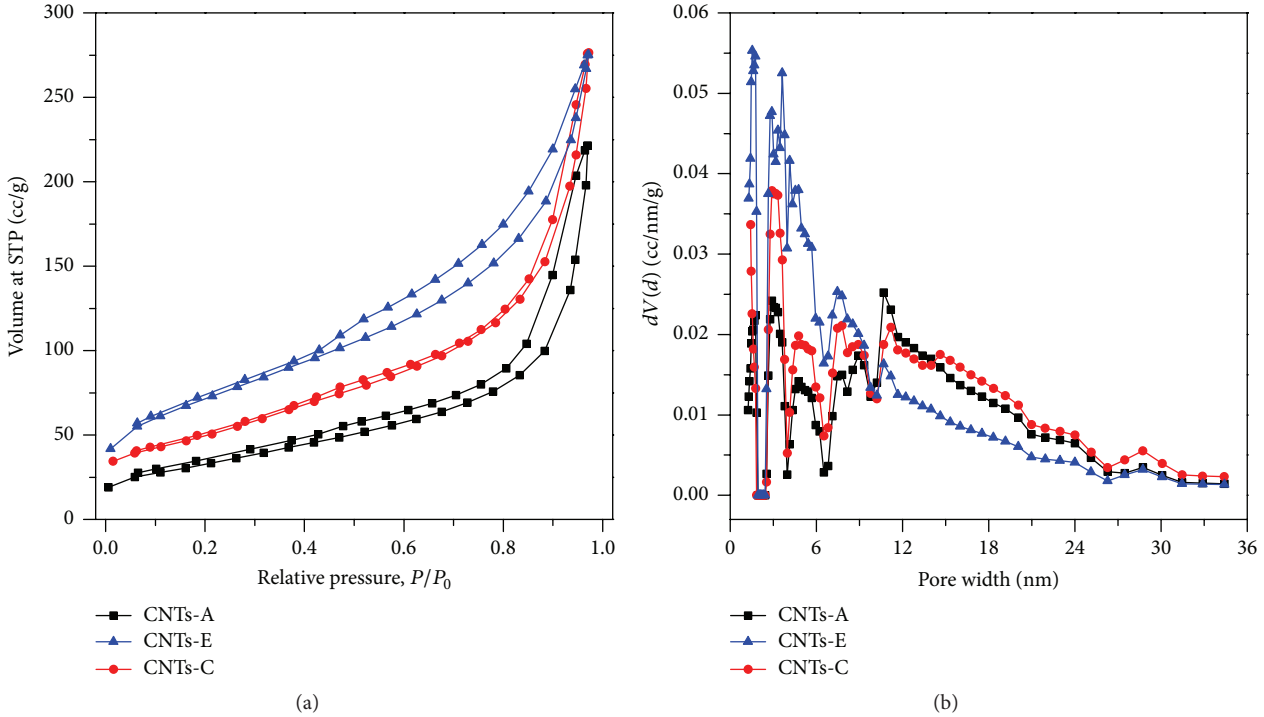

FIGURE 1: N_2 adsorption/desorption isotherms (77 K) (a) and pore size distributions (b) obtained applying the DFT equation corresponding to the CNTs samples.

Table 1 presented the textural parameters for the samples. The variation of carbon sources led to differences in the S_{BET}, total pore volume, and average pore diameter (D_P). Among the samples, the CNTs-E displayed the highest S_{BET} and lowest D_P, indicating that the porosity of CNTs-E was developed. Compared with others, the CNTs-A sample had the lowest S_{BET}, being 65.98% and 46.48% of the CNTs-C and CNTs-E, respectively.

Thermogravimetric analysis (TGA) has been widely used to analyze types of carbon materials. Typically, those losses were attributed to the removal of amorphous carbon (300~400°C), CNTs (400~700°C), and massive graphite carbon (> 700°C). Figure 2(a) showed the weight loss of the purified products during heating in air. Compared with CNTs-A and CNTs-E, the CNTs-C possessed most of the weight loss (97.3%) at 400~700°C, indicating high purity of the CNTs. The weight loss was 90.0%, 91.8%, and 97.3% for CNTs-A, CNTs-E, and CNTs-C, respectively. It was observed that the temperature of initial weight loss was 440°C for CNTs-A, 478°C for CNTs-E, and 618°C for CNTs-C, suggesting that the grown CNTs-C were more highly graphitic with higher initial weight loss temperature.

Raman spectra of the three samples, shown in Figure 2(b), presented a prominent D-band (defects) at 1350 cm^{-1} and a less-intense G-band at 1580 cm^{-1}, attributed to a perfect graphite structure [10, 26, 27]. It was clear that the D-band intensity was higher than the G-band intensity and CNTs-C had a better developed G-band, as well as the D-band. The increase of the G-band relative intensity indicated an improvement of the crystallite orientation, while the increasing D-band relative intensity suggested more defects and an increasing amount of disordered structure of the sample. The pertinent Raman parameter, I_D/I_G, which has already been mentioned to account for the degree of structural order, as displayed in Figure 2(b), confirmed the structure development of the samples (I_D/I_G values of CNTs-A, CNTs-E, and CNTs-C were 1.09, 1.27, and 1.62, resp.).

TABLE 1: Structural characteristics of the studied samples.

Sample	S_{BET} (m^2/g)	V_t (cm^3/g)	Average pore diameter (nm)
CNTs-A	118.1	0.342	11.59
CNTs-C	179.0	0.427	9.55
CNTs-E	254.1	0.425	6.69

3.2. Characterization of Catalysts. The N_2 adsorption/desorption isotherms and pore size distributions were presented in Figure 3. Table 2 summarized the textural parameters for the catalysts. As shown in Figure 3(a), the adsorption volumes of Ni/CNTs were lower than that of Ni/AC owing to the developed microporosity (Figure 3(b)) of AC. When Ni was added into CNTs and AC, the adsorption volumes have decreased for the catalysts, since dispersed Ni was partly embedded into the pores of Ni/CNTs and Ni/AC. Table 2 presented the data for the specific surface areas and total pore volume of the catalysts. The specific surface areas of the catalysts in decreasing order were as follows: Ni/AC > Ni/CNTs-E > Ni/CNTs-C > Ni/CNTs-A. Compared with the

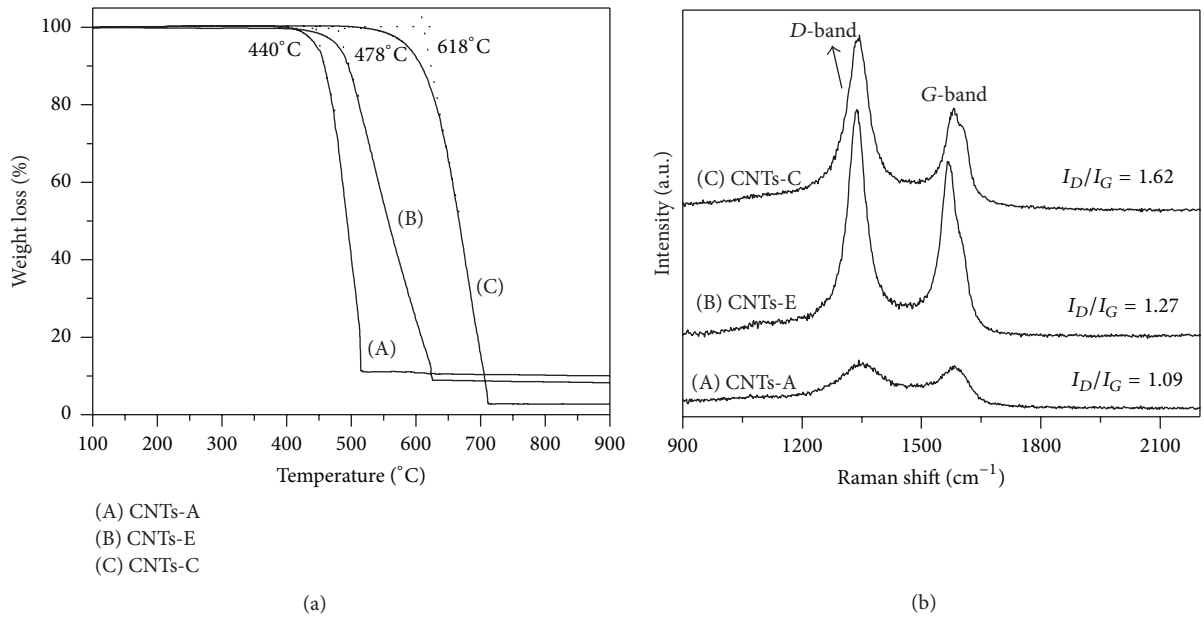

FIGURE 2: TG curves (a) and Raman spectra (b) of the CNTs samples.

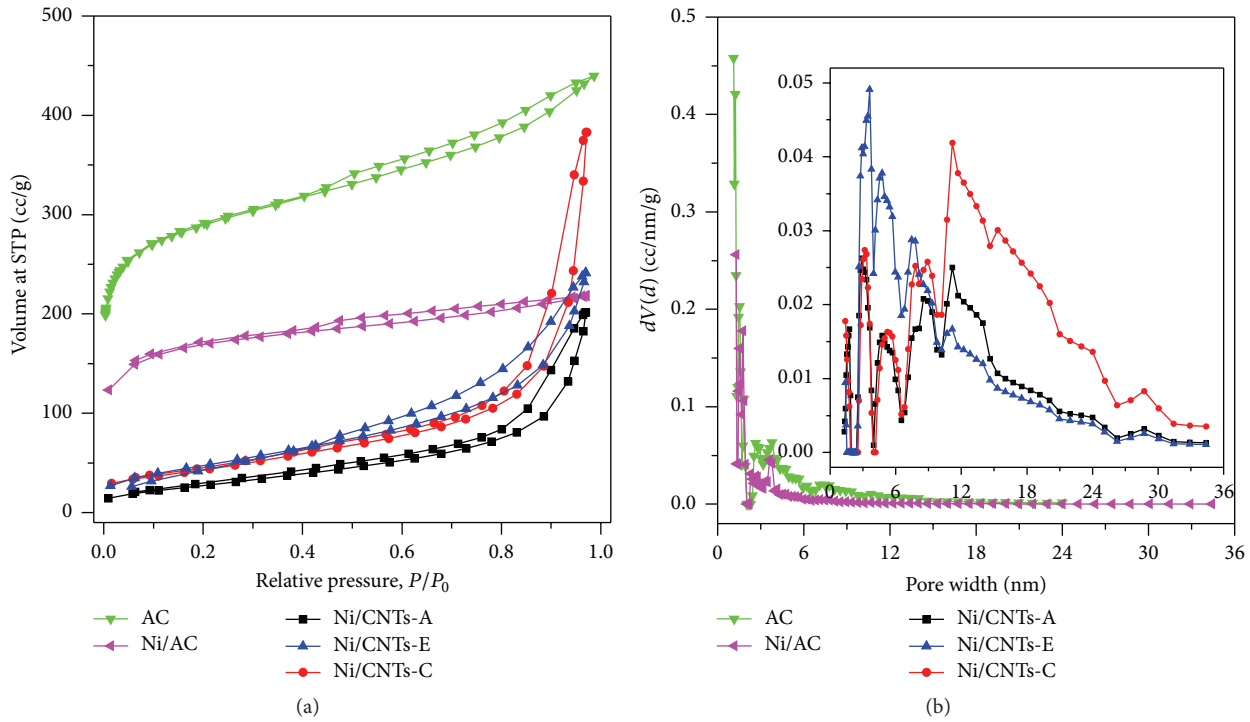

FIGURE 3: N_2 adsorption/desorption isotherms (77 K) (a) and pore size distributions obtained applying the DFT equation (b) corresponding to the catalysts.

other catalysts, the specific surface area of Ni/AC catalyst was decreased significantly due to the existence of Ni. This would result in a low catalytic activity for the CO_2 methanation using Ni/AC as the catalyst.

The XRD analysis was carried out to investigate the crystal structure of the catalyst. As shown in Figure 4, it revealed that the diffraction peak at 26.2° in the catalysts can be well indexed as the (002) reflection of graphite, and the graphite peak of CNTs-supported catalysts was much stronger and narrower than that of the AC-supported catalyst, indicating the crystallinity of CNTs-supported catalysts was high. Metallic Ni species existed in all the reduced samples, with diffraction peaks 44.5°, 51.8°, and 76.5°. According to the crystal plane Ni (111), the particle size of metallic Ni in the

Table 2: Structural characteristics of the catalysts.

Sample	S_{BET} (m^2/g)	V_t (cm^3/g)	Average pore diameter (nm)
AC	927.5	0.680	2.93
Ni/AC	538.4	0.338	2.51
Ni/CNTs-A	103.1	0.312	12.09
Ni/CNTs-C	156.2	0.592	15.17
Ni/CNTs-E	174.7	0.373	8.55

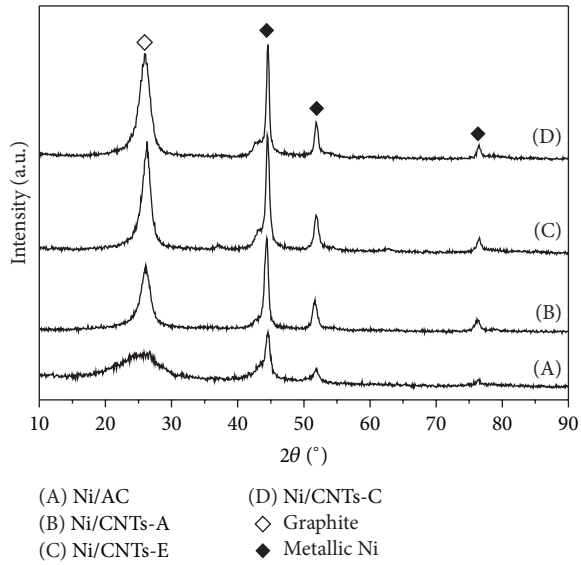

Figure 4: XRD profiles for the reduced catalysts.

catalysts was calculated by Scherrer equation. It was found that the particle size of metallic Ni was 8.9, 9.8, 10.3, and 11.3 nm for Ni/AC, Ni/CNTs-A, Ni/CNTs-E, and Ni/CNTs-C, respectively. Due to the largest specific surface area, AC-supported catalyst was favorable for the decrease of the particle size of Ni.

Temperature-programmed reduction of H_2 (H_2-TPR) is usually employed for estimating reducibility of the catalyst, and the results were displayed in Figure 5. Compared with Ni/AC, the interaction was weaker between CNTs and nickel species for Ni/CNTs series. The low reduction temperatures can be attributed to the overflow effect of hydrogen, which activated hydrogen molecules, thereby promoting the reduction reaction of hydrogen and nickel species at low temperatures. As seen from Figure 5, CNTs-E was to promote the reduction of the nickel species, proved by a significant increase in low temperature reduction.

3.3. Catalytic Performance. The activity of the catalysts was tested by measuring the conversion of CO_2 and the yield of CH_4 as a function of reaction temperature on stream. As shown in Figure 6, except for the catalyst Ni/CNTs-A, the CNTs-supported catalysts displayed better catalytic activity than the AC-supported catalyst, which can be attributed to the high H_2 storage capacity of CNTs, thus promoting

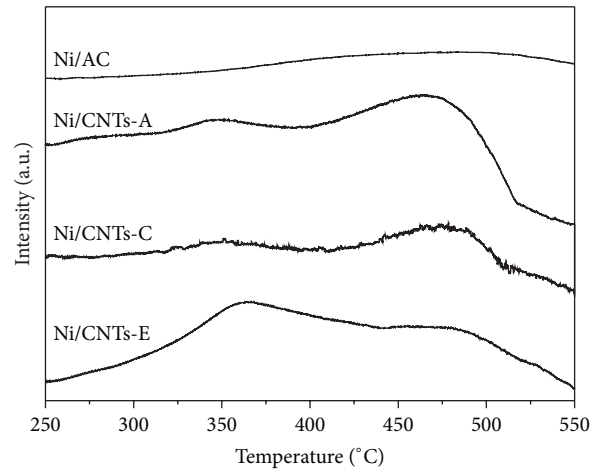

Figure 5: H_2-TPR profiles of the catalysts prepared with different supports.

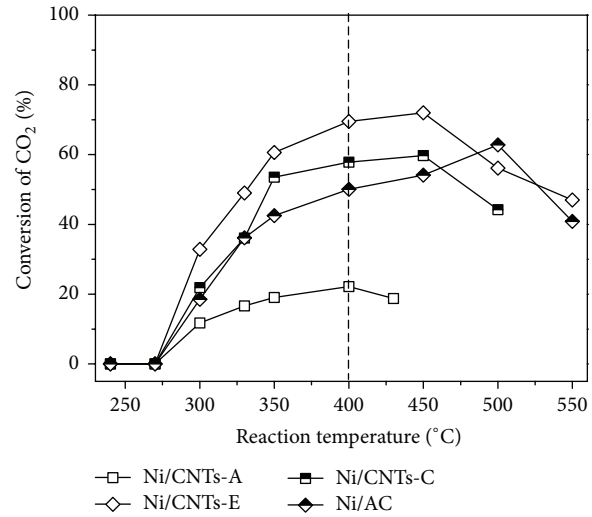

Figure 6: CO_2 conversion versus reaction temperature on the catalysts.

the hydrogenation of CO_2. Compared with Ni/AC, Ni/CNTs-E catalyst had higher catalytic activity, but, with the reaction temperature increasing to 500°C, Ni/CNTs-E had lower catalytic activity than that of Ni/AC. On the whole, the catalytic activity decreased in the following order: Ni/CNTs-E > Ni/CNTs-C > Ni/AC > Ni/CNTs-A.

It revealed that the catalytic activity was improved not only by the specific surface area of the supports, for the specific surface area of CNTs-E, CNTs-C, CNTs-A, and AC was 254.1 m^2/g, 179.0 m^2/g, 118.1 m^2/g, and 927.5 m^2/g, respectively, but also by the overflow effect of hydrogen for CNTs supports. It was observed that the defects over the various CNTs samples have shown no obvious effects on the catalytic activity. For the CNTs supports, CNTs-A had lower defects than CNTs-E and CNTs-C. The catalyst Ni/CNTs-A, with lower defects and specific surface area, showed the lowest catalytic activity among the CNTs-supported samples.

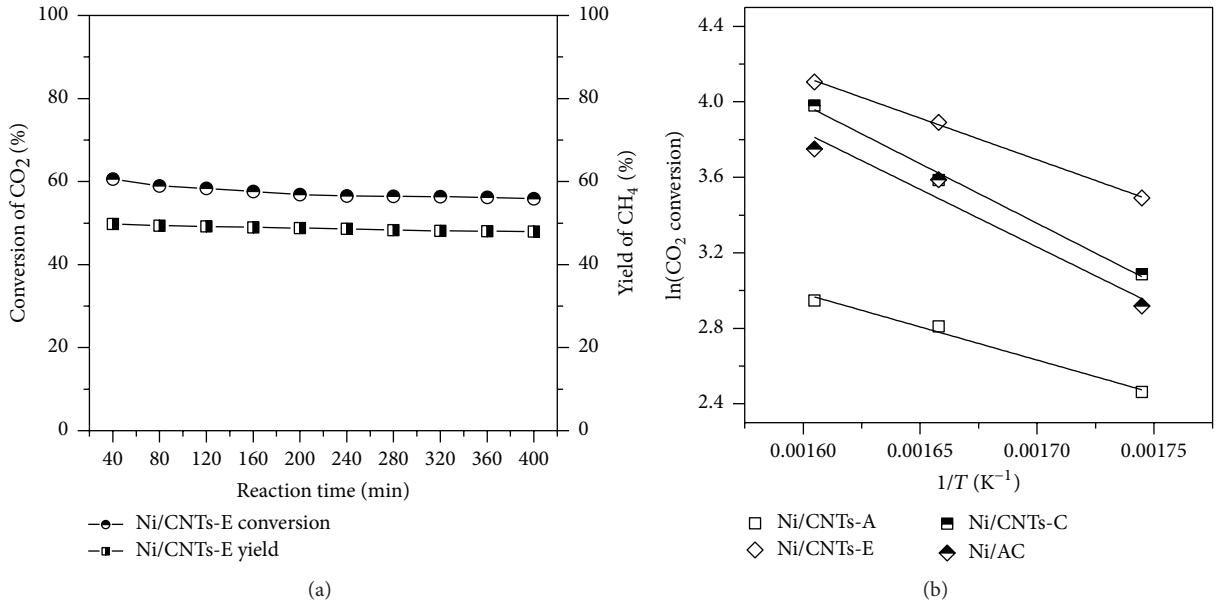

Figure 7: CO_2 conversion and CH_4 yield versus reaction time at 350°C (a) and logarithm of CO_2 conversion versus the reciprocal of temperature (b) on the catalysts.

Herein, for Ni/CNTs-A, the catalytic activity was mainly lowered by the low specific surface area. The CNTs-E and CNTs-C had similar textural properties, but CNTs-C possessed more defects in comparison to CNTs-E. Unexpectedly, the sample Ni/CNTs-C did not exhibit a higher catalytic activity. Hence, compared with the difference in pore structure, the defects played a minor role in catalytic performance of Ni/CNTs for CO_2 methanation.

Figure 7(a) displayed the catalytic stability of the catalyst Ni/CNTs-E. With the reaction proceeding, the catalytic activity decreased slightly, which could be due to sintering of active component. Therefore, it is very important to find the catalyst additives which can improve the stability of the catalyst with low price. Figure 7(b) showed the relationship between logarithm of CO_2 conversion and reciprocal of temperature. Based on Arrhenius formula, activation energies of the catalysts were calculated from the slope of the fitted lines. It was observed that the activation energy decreased for Ni/CNTs-A and Ni/CNTs-E. The activation energies of the catalysts were 29.23, 36.61, 52.54, and 50.77 KJ/mol for Ni/CNTs-A, Ni/CNTs-E, Ni/CNTs-C, and Ni/AC, respectively.

4. Conclusions

The nano Ni-based catalysts supported by CNTs with various textural characteristics were synthetized by impregnation method for CO_2 methanation performance. The prepared CNTs were characterized by N_2 adsorption/desorption, TGA, and Raman spectroscopy, respectively, in order to investigate the textural characteristics of the CNTs. The catalysts were determined by X-ray diffraction (XRD), N_2 adsorption/desorption, and temperature-programmed reduction (H_2-TPR) techniques. The results showed that the textural characteristics of CNTs supports significantly impacted on the catalytic performance of Ni/CNTs, and the catalyst Ni/CNTs-E with good reducibility, large specific surface area, and moderate defects resulted in higher CO_2 conversion and CH_4 yield.

Conflict of Interests

The authors declare that there is no conflict of interests regarding the publication of this paper.

Acknowledgment

This work was supported by the National Basic Research Program of China (973 Program, no. 2011CB201202).

References

[1] F. Ocampo, B. Louis, A. Kiennemann, and A. C. Roger, "CO_2 methanation over Ni-Ceria-Zirconia catalysts: effect of preparation and operating conditions," *IOP Conference Series: Materials Science and Engineering*, vol. 19, no. 1, Article ID 012007, 2011.

[2] S. Eckle, H.-G. Anfang, and R. J. Behm, "What drives the selectivity for CO methanation in the methanation of CO_2-rich reformate gases on supported Ru catalysts?" *Applied Catalysis A: General*, vol. 391, no. 1-2, pp. 325–333, 2011.

[3] S. Sharma, Z. Hu, P. Zhang, E. W. McFarland, and H. Metiu, "CO_2 methanation on Ru-doped ceria," *Journal of Catalysis*, vol. 278, no. 2, pp. 297–309, 2011.

[4] A. Borgschulte, N. Gallandat, B. Probst et al., "Sorption enhanced CO_2 methanation," *Physical Chemistry Chemical Physics*, vol. 15, no. 24, pp. 9620–9625, 2013.

[5] W. Cai, Q. Zhong, and Y. Zhao, "Fractional-hydrolysis-driven formation of non-uniform dopant concentration catalyst nanoparticles of Ni/$Ce_xZr_{1-x}O_2$ and its catalysis in methanation of CO_2," *Catalysis Communications*, vol. 39, pp. 30–34, 2013.

[6] S. Hwang, U. G. Hong, J. Lee et al., "Methanation of carbon dioxide over mesoporous Ni-Fe-Al_2O_3 catalysts prepared by a coprecipitation method: effect of precipitation agent," *Journal of Industrial and Engineering Chemistry*, vol. 19, no. 6, pp. 2016–2021, 2013.

[7] A. Karelovic and P. Ruiz, "CO_2 hydrogenation at low temperature over Rh/γ-Al_2O_3 catalysts: effect of the metal particle size on catalytic performances and reaction mechanism," *Applied Catalysis B: Environmental*, vol. 113-114, pp. 237–249, 2012.

[8] K. Müller, M. Städter, F. Rachow, D. Hoffmannbeck, and D. Schmeißer, "Sabatier-based CO_2-methanation by catalytic conversion," *Environmental Earth Sciences*, vol. 70, no. 8, pp. 3771–3778, 2013.

[9] X. F. Hu, W. Yang, N. Wang, S.-Z. Luo, and W. Chu, "Catalytic properties of Ni/CNTs and Ca-promoted Ni/CNTs for methanation reaction of carbon dioxide," *Advanced Materials Research*, vol. 924, pp. 217–226, 2014.

[10] Y. Y. Feng, C. F. Jiang, D. J. Liu, and W. Chu, "Experimental investigations on microstructure and adsorption property of heat-treated coal chars," *Journal of Analytical and Applied Pyrolysis*, vol. 104, pp. 559–566, 2013.

[11] W. Yang, Y. Y. Feng, and W. Chu, "Comparative study of textural characteristics on methane adsorption for carbon spheres produced by CO_2 activation," *International Journal of Chemical Engineering*, vol. 2014, Article ID 916913, 7 pages, 2014.

[12] A. Karelovic and P. Ruiz, "Mechanistic study of low temperature CO_2 methanation over Rh/TiO_2 catalysts," *Journal of Catalysis*, vol. 301, pp. 141–153, 2013.

[13] F. Ocampo, B. Louis, L. Kiwi-Minsker, and A.-C. Roger, "Effect of Ce/Zr composition and noble metal promotion on nickel based $Ce_xZr_{1-x}O_2$ catalysts for carbon dioxide methanation," *Applied Catalysis A: General*, vol. 392, no. 1-2, pp. 36–44, 2011.

[14] H. Takano, K. Izumiya, N. Kumagai, and K. Hashimoto, "The effect of heat treatment on the performance of the Ni/(Zr-Sm oxide) catalysts for carbon dioxide methanation," *Applied Surface Science*, vol. 257, no. 19, pp. 8171–8176, 2011.

[15] G. Zhi, X. Guo, X. Guo, Y. Wang, and G. Jin, "Effect of La_2O_3 modification on the catalytic performance of Ni/SiC for methanation of carbon dioxide," *Catalysis Communications*, vol. 16, no. 1, pp. 56–59, 2011.

[16] D. C. D. da Silva, S. Letichevsky, L. E. P. Borges, and L. G. Appel, "The Ni/ZrO_2 catalyst and the methanation of CO and CO_2," *International Journal of Hydrogen Energy*, vol. 37, no. 11, pp. 8923–8928, 2012.

[17] A. Beuls, C. Swalus, M. Jacquemin, G. Heyen, A. Karelovic, and P. Ruiz, "Methanation of CO_2: further insight into the mechanism over Rh/γ-Al_2O_3 catalyst," *Applied Catalysis B: Environmental*, vol. 113-114, pp. 2–10, 2012.

[18] C. Swalus, M. Jacquemin, C. Poleunis, P. Bertrand, and P. Ruiz, "CO_2 methanation on Rh/γ-Al_2O_3 catalyst at low temperature: '*in situ*' supply of hydrogen by Ni/activated carbon catalyst," *Applied Catalysis B: Environmental*, vol. 125, pp. 41–50, 2012.

[19] A. Karelovic and P. Ruiz, "Improving the hydrogenation function of Pd/γ-Al_2O_3 catalyst by Rh/γ-Al_2O_3 addition in CO_2 methanation at low temperature," *ACS Catalysis*, vol. 3, no. 12, pp. 2799–2812, 2013.

[20] S. Tada, T. Shimizu, H. Kameyama, T. Haneda, and R. Kikuchi, "Ni/CeO_2 catalysts with high CO_2 methanation activity and high CH_4 selectivity at low temperatures," *International Journal of Hydrogen Energy*, vol. 37, no. 7, pp. 5527–5531, 2012.

[21] W. Yang, W. Chu, C. Jiang, J. Wen, and W. Sun, "Cerium oxide promoted Ni/MgO catalyst for the synthesis of multi-walled carbon nanotubes," *Chinese Journal of Catalysis*, vol. 32, no. 8, pp. 1323–1328, 2011.

[22] W. J. Sun, Z. Q. Liu, C. F. Jiang, Y. Xue, W. Chu, and X. S. Zhao, "Experimental and theoretical investigation on the interaction between palladium nanoparticles and functionalized carbon nanotubes for Heck synthesis," *Catalysis Today*, vol. 212, pp. 206–214, 2013.

[23] J. M. Planeix, N. Coustel, B. Coq et al., "Application of carbon nanotubes as supports in heterogeneous catalysis," *Journal of the American Chemical Society*, vol. 116, no. 17, pp. 7935–7936, 1994.

[24] R. Zacharia, K. Y. Kim, A. K. M. Fazle Kibria, and K. S. Nahm, "Enhancement of hydrogen storage capacity of carbon nanotubes via spill-over from vanadium and palladium nanoparticles," *Chemical Physics Letters*, vol. 412, no. 4–6, pp. 369–375, 2005.

[25] P.-X. Hou, S.-T. Xu, Z. Ying, Q.-H. Yang, C. Liu, and H.-M. Cheng, "Hydrogen adsorption/desorption behavior of multi-walled carbon nanotubes with different diameters," *Carbon*, vol. 41, no. 13, pp. 2471–2476, 2003.

[26] L. Smędowski, M. Krzesińska, W. Kwaśny, and M. Kozanecki, "Development of ordered structures in the high-temperature (HT) cokes from binary and ternary coal blends studied by means of X-ray diffraction and Raman spectroscopy," *Energy & Fuels*, vol. 25, no. 7, pp. 3142–3149, 2011.

[27] Y.-Y. Feng, C.-F. Jiang, D.-J. Liu, and W. Chu, "Microstructure and its influence on CH_4 adsorption behavior of deep coal," *Chinese Physics B*, vol. 23, no. 2, Article ID 028201, 2014.